AGU PUBLICATIONS

Geophysical Research Letters

RESEARCH LETTER
10.1002/2015GL063540

Key Points:
- Observed and simulated satellite tidal magnetic signals agree very well
- Tidal satellite magnetic signals can be used to probe mantle conductivity
- Tidal seafloor EM signals can provide complementary information

Correspondence to:
N. R. Schnepf,
nschnepf@mit.edu

Citation:
Schnepf, N. R., A. Kuvshinov, and T. Sabaka (2015), Can we probe the conductivity of the lithosphere and upper mantle using satellite tidal magnetic signals?, *Geophys. Res. Lett.*, *42*, doi:10.1002/2015GL063540.

Received 17 FEB 2015
Accepted 30 MAR 2015
Accepted article online 8 APR 2015

Can we probe the conductivity of the lithosphere and upper mantle using satellite tidal magnetic signals?

N. R. Schnepf[1], A. Kuvshinov[2], and T. Sabaka[3]

[1]Earth, Atmospheric and Planetary Sciences, MIT, Cambridge, Massachusetts, USA, [2]Institute of Geophysics, ETH Zurich, Zurich, Switzerland, [3]Planetary Geodynamics Laboratory, NASA Goddard Space Flight Center, Greenbelt, Maryland, USA

Abstract A few studies convincingly demonstrated that the magnetic fields induced by the lunar semidiurnal (M2) ocean flow can be identified in satellite observations. This result encourages using M2 satellite magnetic data to constrain subsurface electrical conductivity in oceanic regions. Traditional satellite-based induction studies using signals of magnetospheric origin are mostly sensitive to conducting structures because of the inductive coupling between primary and induced sources. In contrast, galvanic coupling from the oceanic tidal signal allows for studying less conductive, shallower structures. We perform global 3-D electromagnetic numerical simulations to investigate the sensitivity of M2 signals to conductivity distributions at different depths. The results of our sensitivity analysis suggest it will be promising to use M2 oceanic signals detected at satellite altitude for probing lithospheric and upper mantle conductivity. Our simulations also suggest that M2 seafloor electric and magnetic field data may provide complementary details to better constrain lithospheric conductivity.

1. Introduction

Global electromagnetic (EM) studies provide information on mantle electrical conductivity with the ultimate aim of understanding the composition, structure, and dynamics of Earth's interior. For decades these studies were based on interpretation of magnetic data from a global network of observatories (*Banks* [1969], *Schultz and Larsen* [1987], *Olsen* [1998], *Schmucker* [1999], *Kelbert et al.* [2009], *Semenov and Kuvshinov* [2012], and *Koyama et al.* [2014], among many others). The recent expansion in magnetic data from low-Earth orbiting satellite missions (Oersted, CHAMP, SAC-C, and *Swarm*) has led to a rising interest in probing Earth from space [*Kuvshinov and Olsen*, 2006; *Velímský*, 2010, 2013; *Civet and Tarits*, 2013; *Püthe and Kuvshinov*, 2013, 2014]. For example, mapping the electrical conductivity of Earth's mantle was assigned to be one of the primary scientific objectives of *Swarm* [*Olsen et al.*, 2013]. The largest benefit of using satellite data is much improved spatial coverage. Additionally, and in contrast to ground-based data, satellite data are overall uniform and very high quality.

The main source exploited by either ground-based or satellite global EM studies is the magnetospheric ring current. Variations due to this source are in the period range of a few days to a few months, and thus, in accordance to the skin depth concept these data are most sensitive to conductivity structures at mid mantle depths (400–1500 km).

At the same time, there is great interest in mapping the conductivity in the lithosphere and upper mantle (LUM), i.e., depths between 10 and 400 km. Recent laboratory experiments demonstrate that the electrical conductivity of LUM minerals is greatly affected by small amounts of water or by partial melt (*Wang et al.* [2006], *Gaillard et al.* [2008], and *Yoshino et al.* [2009], among others). Determination of LUM conductivity using EM methods can thus provide constraints on melting processes and the presence of water in LUM. However, probing the conductivity at these shallower depths requires EM variations with periods of a few hours. This is a challenging period range for global EM studies since the ionospheric (Sq) source, which dominates these periods, has a much more complex spatial structure compared to the magnetospheric ring current.

Fortunately, there exists an alternative EM source in the Sq period range—electric currents generated by oceanic tides. This source arises from a simple geophysical process: as electrically conducting salt water moves through the ambient magnetic field of the Earth, it generates secondary magnetic and electric fields. The EM signals due to (periodic) tidal sources can be most easily detected either at seafloor [*Kuvshinov et al.*, 2006; *Schnepf et al.*, 2014] or coastal stations [*Maus and Kuvshinov*, 2004; *Love and Rigler*, 2014]. Unlike the

Sq signals, the EM signals produced from ocean tides galvanically couple with the Earth's subsurface. The Sq current system is not in electrical (galvanic) contact with the Earth due to the insulating atmosphere, so the electric currents induced in a 1-D Earth are always horizontal (i.e., toroidal electric currents) and consequently are insensitive to regions with a lower conductivity than their surroundings. In a 3-D Earth (for example, picture the Earth having inhomogeneous oceans and a 1-D underlying mantle), resistive regions can only be imaged indirectly through the deviation of an electric current into conductive material. Thus, the physics behind this intrinsically biases results of EM sensing with the use of Sq data toward conductive zones within the Earth. However, resistive zones (which are mostly associated with the lithosphere and upper mantle) may be of considerable geodynamic interest. For example, regions with deficiencies of partial melts and/or volatiles will be quite resistive.

Because the oceanic tidal current system is in galvanic contact with the underlying media, the tidal source induces both poloidal and toroidal electric currents. This occurs even in a 1-D Earth where poloidal electric currents involve the vertical component. However, it is known [e.g., *Fainberg et al.*, 1990] that the poloidal electric currents are preferentially sensitive to resistive structures and thus so are EM signals of oceanic tidal origin.

In order to probe the Earth using either Sq or oceanic tidal signals, the source of these signals must first be specified as accurately as possible. Recall that the Sq source can be represented as an electric current system flowing in an ionospheric shell at a height of around 110 km, whereas the oceanic tidal source can be represented as an electric current system flowing in the oceans. It is well known that the oceanic tidal electric current at any location is proportional to the cross (vector) product of the velocity and main magnetic field, which both are now determined with unprecedented accuracy. In particular, this means that the tidal source is also determined very accurately. It is important to stress that the tidal source determination does not rely on the tidal EM (either satellite or ground-based) data that are used for probing the Earth. Indeed, the main magnetic field and the tidal velocity are determined from independent data. With a known tidal source, Earth's conductivity may be constrained by fitting observed and predicted tidal EM signals.

The situation for the Sq source is different. The Sq source is determined from the EM data that are intended to probe the Earth. When using global ground-based data, the Sq source is conventionally recovered using the potential method. The potential method—as applied to global ground-based data—allows for separating internal and external parts of the magnetic potential by exploiting the least squares technique and spherical harmonic representation. Once the external part is estimated, the ionospheric Sq current system may be reconstructed. With a known Sq source, Earth's conductivity may be constrained by fitting observed and predicted Sq signals. Unfortunately, this scheme only works with ground-based data. When using satellite Sq data, because satellites fly far above the ionospheric shell, the Sq signals are seen as purely internal and thus the separation of satellite Sq signals into internal and external parts is not possible.

Tyler et al. [2003] and *Sabaka et al.* [2015] convincingly demonstrated that magnetic fields induced by the lunar semidiurnal (M2) ocean flow can be identified in nighttime magnetic satellite observations. Figure 1 shows the predicted M2 radial magnetic field and that recovered by *Sabaka et al.* [2015] using over 12 years of data from CHAMP, Oersted, and SAC-C. One immediately sees that observations and simulations (to be discussed in the next sections) agree very well. This result supports the idea to use M2 satellite magnetic data for constraining LUM electrical conductivity.

In this paper, we perform global 3-D EM numerical simulations in order to quantitatively investigate the actual sensitivity of M2 tidal signals to conductivity distributions at different depths. Note that because we are only discussing M2 tidal signals, this is different than EM-sounding studies where the aim is to determine conductivity as a function of different frequencies. Considering (1) the long period of M2 variations (12.4206 h); (2) the galvanic excitation of the Earth from the M2 tidal current, and (3) the rich spatial content of the M2 source [cf. *Sabaka et al.*, 2015, Figure 11], this type of Earth probing is a form of geoelectric sounding analogous with the direct current (DC) electric sounding method. The latter method is based on DC or low-frequency current injection through grounded electrodes (galvanic excitation). It is known that the depth of DC sounding depends on the distance between the electrodes. In the case of the M2 ocean tide, the different spatial scales of the M2 source may be related to the different distances between electrodes in DC sounding. This enables sensing conductivity at different depths.

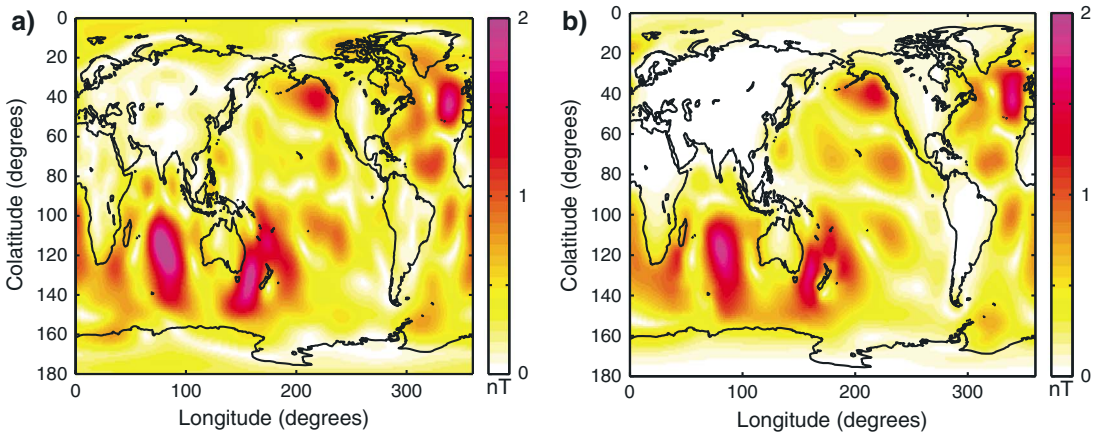

Figure 1. The amplitude of the M2 radial magnetic signals at satellite height from (a) CM5 [see *Sabaka et al.*, 2015] and (b) our study's simulation using HAMTIDE for the tidal velocity source.

2. Forward Simulation of the M2 EM Signals

We simulate EM signals due to the M2 oceanic tidal flow (period of 12.4206 h) using the frequency-domain numerical solution described in *Kuvshinov* [2008]. This solution computes the electric (**E**) and magnetic (**B**) fields excited by an electric source in spherical models of the Earth with a three-dimensional (3-D) distribution of electrical conductivity. Within this solution, Maxwell's equations in the frequency domain,

$$\frac{1}{\mu_0}\nabla \times \mathbf{B} = \sigma \mathbf{E} + \mathbf{j}^{\text{ext}} \tag{1}$$

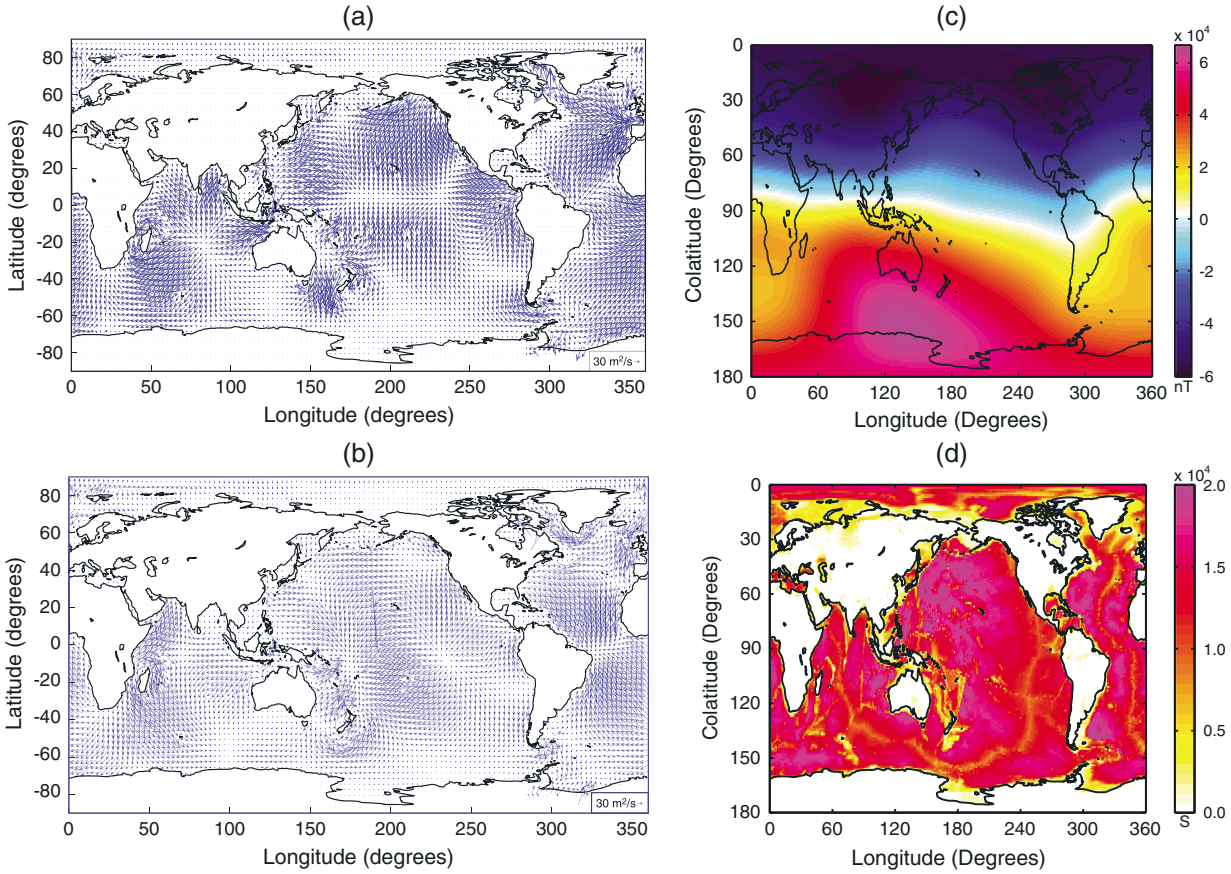

Figure 2. The (a) real and (b) imaginary velocity vectors for the depth-integrated M2 tidal velocities (m^2/s) produced by HAMTIDE, as well as (c) the radial main field (nT) from WMM for the year 2014 and (d) the ocean conductance (S) map.

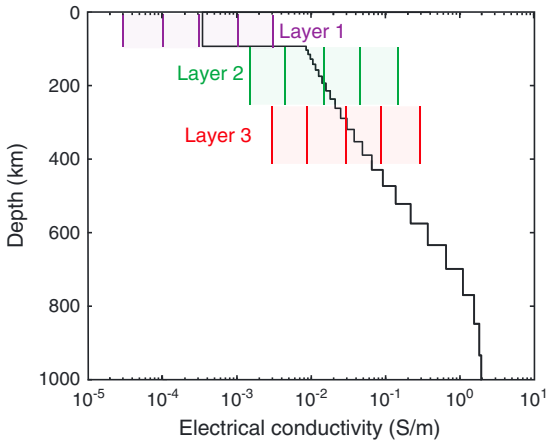

Figure 3. The five conductivity values used for layer 1 (purple), layer 2 (green), and layer 3 (red) are shown in vertical lines that span the layers' depth. Below the three layers, the black line depicts the conductivity profile from *Kuvshinov and Olsen* [2006].

and

$$\nabla \times \mathbf{E} = i\omega \mathbf{B}\,, \tag{2}$$

are reduced to an integral equation (IE) with a contracting kernel [e.g., *Pankratov et al.*, 1995]. Here $\mathbf{j}^{\text{ext}}$ is the complex-valued impressed current (in our case, $\mathbf{j}^{\text{ext}}$ is the electric current induced by the tidal flow), σ is the conductivity distribution of the model, μ_0 is the magnetic permeability of the free space, and ω is an angular frequency. After solving the IE, the electric and magnetic fields at the observation points are calculated using Green's function formalism. For a detailed description of the 3-D EM simulation as applied to motionally induced signals, see *Kuvshinov and Olsen* [2004] and *Kuvshinov* [2008]. The impressed current, $\mathbf{j}^{\text{ext}}$, is calculated as

$$\mathbf{j}^{\text{ext}} = \sigma_w \left(\mathbf{U} \times \mathbf{B}^m\right)\,, \tag{3}$$

where σ_w = 3.2 S/m is the mean seawater conductivity, $\mathbf{U}$ is the complex-valued depth-integrated velocity due to ocean tides, and $\mathbf{B}^m$ is the (ambient) main magnetic field of internal origin. Two assimilated tidal models of $\mathbf{U}$ were tried during simulations: the 0.25° × 0.25° resolution global tidal model TPX07.2 [*Egbert and Erofeeva*, 2002] and the 0.125° × 0.125° resolution global tidal model HAMTIDE (shown in Figures 2a and 2b) [*Taguchi et al.*, 2014]. The ambient magnetic field was derived from the World Magnetic Model (WMM) [*Chulliat et al.*, 2015]. Figure 2c shows the radial component of the main field which is determinative in specifying $\mathbf{j}^{\text{ext}}$. The 3-D model consisted of a thin spherical layer of laterally varying conductance at the Earth's surface (shown in Figure 2d) and a radially symmetric spherical conductivity underneath (shown in Figure 3). The surface conductance distribution was taken from *Manoj et al.* [2006] and accounts for the contributions from seawater and sediments. For the underlying laterally homogeneous spherical conductor, we used the model of *Kuvshinov and Olsen* [2006] as the default scenario (more explanation is provided in the following section). The 1° × 1° simulations were performed at the seafloor, sea level, and satellite height (430 km altitude). Note that since we observed only negligible differences between the simulations which used the HAMTIDE and TPXO7.2 models for the tidal velocity (which was unsurprising since their tidal velocity models were quite similar), for the rest of our analysis we focus on the results that used the HAMTIDE velocity model.

3. Sensitivity Analysis

A simple analysis was done to gauge the sensitivity of the M2 tidal signal to changes in lithospheric and mantle conductivity. As specified in Table 1 and Figure 3, we varied the conductivity in the lithospheric layer (10–100 km) and the following two upper mantle layers (depths of 101–250 km and 251–410 km) to simulate magnetic and electric fields for cases of greater/lower conductivity value. The depths of these layers were determined from seismic data—100 km marks the base of lithosphere and the transition zone starts at 410 km. We broke the upper mantle before the transition zone into two layers in a manner similar to *Kelbert et al.* [2008] and used 250 km as the midpoint between the two layers. The range of conductivity values used in each layer is based on the results of deep EM studies which are supported by laboratory conductivity measurements compiled in *Khan and Shankland* [2012] and partially updated in *Koyama et al.* [2014].

For each simulation run, only one layer's conductivity was varied while the other two layers were held at the default conductivity value from *Kuvshinov and Olsen* [2006] (cf. Table 1). In this way, the sensitivity of M2

Table 1. Trial Conductivities of Lithosphere and Upper Mantle Layers Used During the Simulation

	Conductivity Values (S/m)				
Depth of Layer	C1	C2	C3[a]	C4	C5
Layer 1: 10–100 km	0.003	0.001	0.0003	0.0001	0.00003
Layer 2: 101–250 km	0.16	0.05	0.016	0.005	0.0016
Layer 3: 251–410 km	0.3	0.1	0.03	0.01	0.003

[a]Column (C3) that contains conductivities recovered by *Kuvshinov and Olsen* [2006].

oceanic tidal signals to the conductivity of a specific layer (i.e., sensitivity to depth) was determined. Figure 4 shows the results of the sensitivity analysis at satellite height and at the seafloor. The analysis was done for the radial magnetic field component and for the horizontal magnetic and electric field components. The plots show the Frobenius norm of the differences between the results obtained from conductivity scenario C1 versus scenarios C2, C3, C4, and C5 for each layer:

$$||S^{l,k}||_F = \left(\sum_{i,j} |F_{ij}^{l,k} - F_{ij}^{l,1}|^2 \right)^{1/2}, \tag{4}$$

where F denotes the corresponding field component, i, j labels grid points in or above oceanic regions, k represents the conductivity scenario (C1, C2, C3, C4, or C5) and l denotes the layer being analyzed. Note that in Figure 4 the results for the first, second, and third layers are depicted by red, blue, and black colors, respectively. In all layers the range of conductivity changes was 2 orders of magnitude. Figures 4a and 4b show the results of the sensitivity analysis at satellite height. The electric field at satellite height is not shown because this field is of telluric origin and is not measured by satellites. The maximum sensitivity is detected from conductivity changes in the first upper mantle layer (101–250 km), and the minimum sensitivity is mostly due to changes in the second upper mantle layer (251–410 km). It is also seen that with decreasing conductivity the curves flatten; however, for all scenarios and layers, changing the conductivity from C2 to C3 (three times

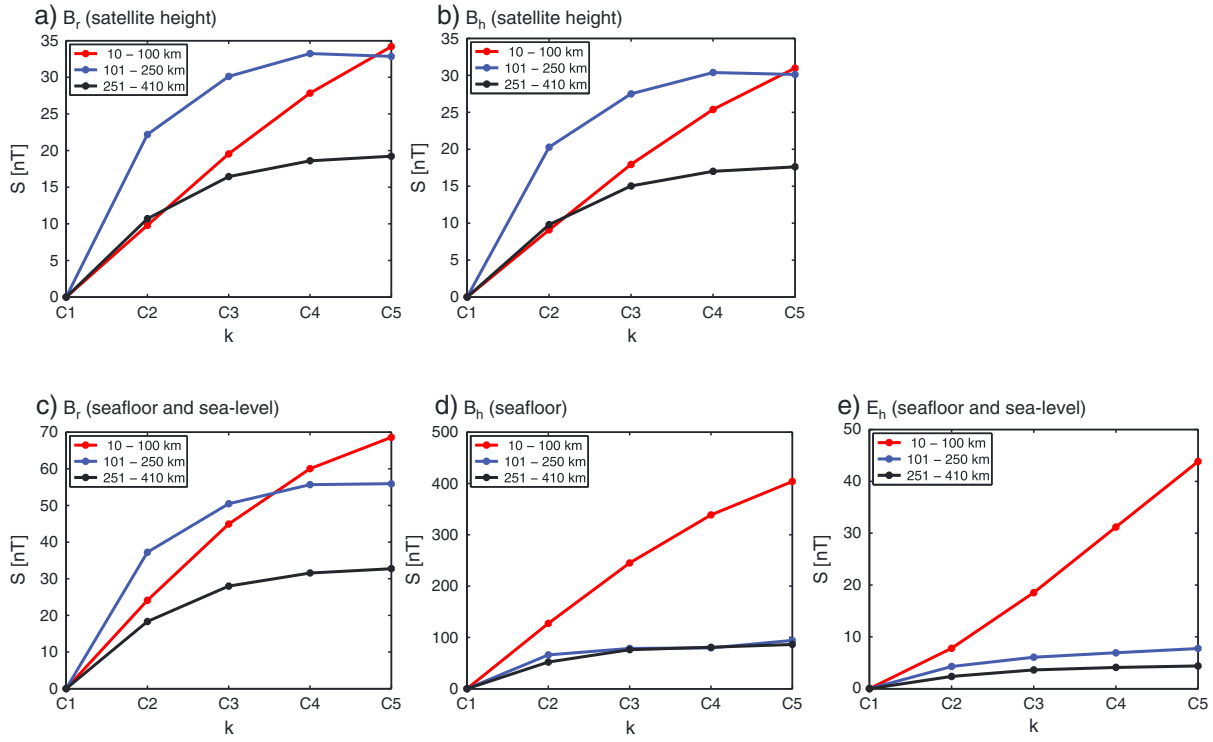

Figure 4. Results of the sensitivity analysis. Frobenius norms for (a) the radial magnetic field component and (b) the horizontal magnetic field component at satellite height, as well as (c) the seafloor and sea level radial magnetic field component, (d) the seafloor horizontal magnetic field component, and (e) the seafloor and sea level horizontal electric field.

changed) leads to a significant (up to twofold) increase of $||S||_F$. This suggests that M2 satellite magnetic signals can be used to probe the conductivity of the lithosphere and upper mantle. The overall behavior of $||S||_F$ for radial (Figure 4a) and horizontal (Figure 4b) magnetic field components at satellite height is very similar. This, in particular, means that above the Earth the horizontal magnetic field component does not add any new information about the Earth's conductivity.

Figures 4c–4e show the results of the sensitivity analysis at the seafloor. Note that the radial magnetic field and horizontal electric field components are the same at sea level and the seafloor. The behavior of $||S||_F$ in the radial component at satellite height and at sea level (cf. leftmost plots) is very similar, with the main differences being that $||S||_F$ at sea level is about two times larger than $||S||_F$ at satellite height and the lithospheric sensitivity surpasses that of the upper mantle at k = C4,C5. More dramatic changes in $||S||_F$ occur in the horizontal magnetic field component at the seafloor compared with that at satellite height. First, $||S||_F$ at the sea floor is over 10 times larger than $||S||_F$ at satellite height. Second, the horizontal magnetic field appears to be most sensitive to conductivity changes in the lithospheric layer (10–100 km). The same is true for the horizontal electric field, as it shows even larger sensitivity to lithospheric conductivity. This suggests that the seafloor magnetic and electric field data (such as those used by *Toh et al.* [2006], *Baba et al.* [2010], *Baba et al.* [2013], and *Schnepf et al.* [2014]) could provide complementary insights on lithospheric conductivity.

4. Concluding Remarks

Our sensitivity analysis of oceanic M2 tidal EM signals suggests it will be promising for future studies to use M2 oceanic signals to probe lithospheric and upper mantle conductivity. Our analysis also suggests that seafloor magnetic and electric data can provide complementary details to better determine lithospheric conductivity. Note that there also exists a few more tidal modes of similar periodicity (for example, O1 or N2) but they are at least 1 order of magnitude smaller, thus, making their identification from satellite EM data more problematic.

We have to stress that there are some strong advantages of working with oceanic tidal signals. First, the spatial structure of the tidal source is determined more accurately compared with the ionospheric Sq source. Second, in contrast to Sq signals, the oceanic tidal signals—being of gravitational origin—do not undergo day-to-day and seasonal variabilities and, moreover, do not depend on solar activity as the Sq signals do. Due to the direct galvanic coupling of the source (electric currents in the ocean) with the subsurface structures, tidal signals are more sensitive than Sq signals to shallower and less conductive structures. Sq signals, instead, undergo inductive coupling between the source and subsurface. However, working with tidal signals also has some shortcomings, for example, in contrast to the global Sq source, the tidal source is confined only to oceanic regions. Arguably, because there is a relative lack of observatories in oceanic regions, this disadvantage is in fact filling in a needed knowledge gap in investigating the oceanic lithosphere and upper mantle.

Finally, we would like to note that the next natural step of the research would be inverting the recovered tidal signals (as well as those yet to be recovered from *Swarm* data) in terms of LUM conductivity (either in the frame of a 1-D or 3-D model). This will be a topic of our forthcoming publication.

Acknowledgments

N.R.S. would like to thank the NSF Graduate Research Fellowship Program for support. The CM5 data used here may be obtained by contacting T. J. Sabaka (terence.j.sabaka@nasa.gov) and the model output may be obtained by contacting N. R. Schnepf (nschnepf@mit.edu).

The Editor thanks two anonymous reviewers for their assistance in evaluating this paper.

References

Baba, K., H. Utada, T.-N. Goto, T. Kasaya, H. Shimizu, and N. Tada (2010), Electrical conductivity imaging of the Philippine Sea upper mantle using seafloor magnetotelluric data, *Phys. Earth Planet. Inter.*, *183*(1-2), 44–62, doi:10.1016/j.pepi.2010.09.010.

Baba, K., N. Tada, L. Zhang, P. Liang, H. Shimizu, and H. Utada (2013), Is the electrical conductivity of the northwestern Pacific upper mantle normal?, *Geochem. Geophys. Geosyst.*, *14*, 4969–4979, doi:10.1002/2013GC004997.

Banks, R. J. (1969), Geomagnetic variations and the conductivity of the upper mantle, *Geophys. J. Int.*, *17*, 457–487.

Chulliat, A., S. Macmillan, P. Alken, C. Beggan, M. Nair, B. Hamilton, A. Woods, V. Ridley, S. Maus, and A. Thomson (2015), The US/UK world magnetic model for 2015–2020, *Tech. Rep.*, NOAA National Geophysical Data Center, Boulder, Colo., doi:10.7289/V5TH8JNW.

Civet, F., and P. Tarits (2013), Analysis of magnetic satellite data to infer the mantle electrical conductivity of telluric planets in the solar system, *Planet. Space Sci.*, *84*, 102–111, doi:10.1016/j.pss.2013.05.004.

Egbert, G. D., and S. Y. Erofeeva (2002), Efficient inverse modeling of barotropic ocean tides, *J. Atmos. Oceanic Technol.*, *19*, 183–204.

Fainberg, E. B., A. V. Kuvshinov, and B. S. Singer (1990), Electromagnetic induction in a spherical Earth with nonuniform oceans and continents in electric contact with the underlying medium: 2. Bimodal global geomagnetic sounding of the lithosphere, *Geophys. J. Int.*, *102*, 273–281, doi:10.1016/0198-0254(88)92599-X.

Gaillard, F., M. Malki, G. Iacono-Marziano, M. Pichavant, and B. Scaillet (2008), Carbonatite melts and electrical conductivity in the asthenosphere, *Science*, *322*, 1363–1365, doi:10.1126/science.1164446.

Kelbert, A., G. D. Egbert, and A. Schultz (2008), Non-linear conjugate gradient inversion for global EM induction: Resolution studies, *Geophys. J. Int.*, *173*(2), 365–381, doi:10.1111/j.1365-246X.2008.03717.x.

Kelbert, A., A. Schultz, and G. Egbert (2009), Global electromagnetic induction constraints on transition-zone water content variations, *Nature*, *460*, 1003–1006, doi:10.1038/nature08257.

Khan, A., and T. J. Shankland (2012), A geophysical perspective on mantle water content and melting: Inverting electromagnetic sounding data using laboratory-based electrical conductivity profiles, *Earth Planet. Sci. Lett.*, *317-318*, 27–43, doi:10.1016/j.epsl.2011.11.031.

Koyama, T., A. Khan, and A. Kuvshinov (2014), Three-dimensional electrical conductivity structure beneath Australia from inversion of geomagnetic observatory data: Evidence for lateral variations in transition-zone temperature, water content and melt, *Geophys. J. Int.*, *196*, 1330–1350, doi:10.1093/gji/ggt455.

Kuvshinov, A., and N. Olsen (2004), 3-D modelling of the magnetic fields due to ocean tidal flow, in *CHAMP Mission Results II*, pp. 359–365, Springer, Berlin.

Kuvshinov, A., and N. Olsen (2006), A global model of mantle conductivity derived from 5 years of CHAMP, Ørsted, and SAC-C magnetic data, *Geophys. Res. Lett.*, *33*, L18301, doi:10.1029/2006GL027083.

Kuvshinov, A., A. Junge, and H. Utada (2006), 3-D modelling the electric field due to ocean tidal flow and comparison with observations, *Geophys. Res. Lett.*, *33*, L06314, doi:10.1029/2005GL025043.

Kuvshinov, A. V. (2008), 3-D global induction in the oceans and solid earth: Recent progress in modeling magnetic and electric fields from sources of magnetospheric, ionospheric and oceanic origin, *Surv. Geophys.*, *29*(2), 139–186, doi:10.1007/s10712-008-9045-z.

Love, J. J., and E. J. Rigler (2014), The magnetic tides of Honolulu, *Geophys. J. Int.*, *197*, 1335–1353, doi:10.1093/gji/ggu090.

Manoj, C., A. Kuvshinov, S. Maus, and H. Luhr (2006), Ocean circulation generated signals, *Earth Planets Space*, *58*, 429–437.

Maus, S., and A. Kuvshinov (2004), Ocean tidal signals in observatory and satellite magnetic measurements, *Geophys. Res. Lett.*, *31*, L15313, doi:10.1029/2004GL020090.

Olsen, N. (1998), The electrical conductivity of the mantle beneath Europe derived from C-responses from 3 to 720 hr, *Geophys. J. Int.*, *133*, 298–308.

Olsen, N., et al. (2013), The Swarm Satellite Constellation Application and Research Facility (SCARF) and Swarm data products, *Earth Planets Space*, *65*(c), 1189–1200, doi:10.5047/eps.2013.07.001.

Pankratov, O., D. Avdeev, and A. Kuvshinov (1995), Electromagnetic field scattering in a homogeneous Earth: A solution to the forward problem, *Phys. Solid. Earth*, *31*, 201–209.

Püthe, C., and A. Kuvshinov (2013), Determination of the 3-D distribution of electrical conductivity in Earth's mantle from Swarm satellite data: Frequency domain approach based on inversion of induced coefficients, *Earth Planets Space*, *65*, 1247–1256, doi:10.5047/eps.2013.09.004.

Püthe, C., and A. Kuvshinov (2014), Mapping 3-D mantle electrical conductivity from space: A new 3-D inversion scheme based on analysis of matrix Q-responses, *Geophys. J. Int.*, *197*, 768–784, doi:10.1093/gji/ggu027.

Sabaka, T. J., N. Olsen, R. H. Tyler, and A. Kuvshinov (2015), CM5, a pre-Swarm comprehensive geomagnetic field model derived from over 12 yr of CHAMP, Orsted, SAC-C and observatory data, *Geophys. J. Int.*, *200*, 1596–1626, doi:10.1093/gji/ggu493.

Schmucker, U. (1999), A spherical harmonic analysis of solar daily variations in the years 1964–65—I. Methods, *Geophys. J. Int.*, *136*, 439–454.

Schnepf, N. R., C. Manoj, A. Kuvshinov, H. Toh, and S. Maus (2014), Tidal signals in ocean bottom magnetic measurements of the Northwestern Pacific: Observation versus prediction, *Geophys. J. Int.*, *198*(2), 1096–1110.

Schultz, A., and J. C. Larsen (1987), On the electrical conductivity of the mid-mantle—I. Calculation of equivalent scalar magnetotelluric response functions, *Geophys. J. Int.*, *88*, 733–761.

Semenov, A., and A. Kuvshinov (2012), Global 3-D imaging of mantle conductivity based on inversion of observatory C-responses-II. Data analysis and results, *Geophys. J. Int.*, *191*, 965–992, doi:10.1111/j.1365-246X.2012.05665.x.

Taguchi, E., D. Stammer, and W. Zahel (2014), Inferring deep ocean tidal energy dissipation from the global high-resolution data-assimilative HAMTIDE model, *J. Geophys. Res. Oceans*, *119*, 4573–4592, doi:10.1002/2013JC009766.

Toh, H., Y. Hamano, and M. Ichiki (2006), Long-term seafloor geomagnetic station in the northwest Pacific: A possible candidate for a seafloor geomagnetic observatory, *Earth Planets Space*, *58*, 697–705.

Tyler, R. H., S. Maus, and H. Lühr (2003), Satellite observations of magnetic fields due to ocean tidal flow, *Science*, *299*(5604), 239–241, doi:10.1126/science.1078074.

Velímský, J. (2010), Electrical conductivity in the lower mantle: Constraints from CHAMP satellite data by time-domain EM induction modelling, *Phys. Earth Planet. Inter.*, *180*, 111–117, doi:10.1016/j.pepi.2010.02.007.

Velímský, J. (2013), Determination of three-dimensional distribution of electrical conductivity in the Earth's mantle from Swarm satellite data: Time-domain approach, *Earth Planets Space*, *65*, 1239–1246, doi:10.5047/eps.2013.08.001.

Wang, D., M. Mookherjee, Y. Xu, and S.-I. Karato (2006), The effect of water on the electrical conductivity of olivine, *Nature*, *443*, 977–980, doi:10.1038/nature05256.

Yoshino, T., T. Matsuzaki, A. Shatskiy, and T. Katsura (2009), The effect of water on the electrical conductivity of olivine aggregates and its implications for the electrical structure of the upper mantle, *Earth Planet. Sci. Lett.*, *288*, 291–300, doi:10.1016/j.epsl.2009.09.032.